JAM CM Journal of Applied Mathematics and Computational Mechanics 2022, 21(2), 77-90
www.amcm.pcz.pl p-ISSN 2299-9965
DOI: 10.17512/jamcm.2022.2.07 e-ISSN 2353-0588

# MAGNETOCONVECTION OF NANOFLUID IN A PARTIALLY HEATED CAVITY WITH ISOTHERMAL BLOCKAGE

***Suresh Nagaraj*[1], *Nithyadevi Nagarajan*[2]**

[1] *Department of Mathematics, Bharathiar University*
*Coimbatore, India*
[2] *Department of Applied Mathematics, Bharathiar University*
*Coimbatore, India*
*suresh.n991@buc.edu.in, nithyadevin@buc.edu.in*

Received: 19 November 2021; Accepted: 21 January 2022

**Abstract.** Natural convection characteristics of $Al_2O_3$-water nanofluid in a cavity is investigated numerically under the influence of a inclined magnetic field. The bottom wall is partially heated, and the top wall is cooled and the remaining regions of the cavity are kept adiabatic. An isothermally heated square blockage of the different rectangular size is placed at the centre of the cavity. The schematic model is converted into mathematical form, and the non-dimensional equations are discretized by the finite volume method using power law scheme and solved by Semi-Implicit Method for Pressure Linked Equation algorithm. The relevant parameters such as Rayleigh number ($10^4$-$10^6$), Hartmann number (10-500), size of blockage ratio (0.25-0.75), length of the heat source (0.25-1.0) and inclination angle of the magnetic field ($0^\circ$-$90^\circ$) on the flow and temperature fields are examined. Results are presented in terms of streamlines, isotherms, velocity profile, local and average Nusselt number. It was found that for low Hartmann numbers, the average heat transfer rate attained the maximum at the inclined magnetic field of $\gamma = 45^\circ$. In addition, the blockage ratio of B = 0.75 enhanced the higher heat transfer rate for all values of $\gamma$.

***MSC 2010:*** *76M12, 80M12, 80A20, 35Q79*
***Keywords:*** *$Al_2O_3$ nanofluid, finite volume method, inclined magnetic field, isothermal square body, natural convection, partial bottom heating*

## 1. Introduction

Natural convective heat transfer influenced by the temperature gradient across the walls of cavity has significant practical and industrial applications such as in heating and cooling of buildings [1], electronic devices, glazing units used in buildings, cooling of containers and heat exchangers, solar energy collectors, energy drying processes, solar distillers [2], etc. In the study of natural convection, the configuration bounded by adiabatic vertical walls and differentially heated horizontal walls with bottom wall maintained with higher temperature is referred to as classical Rayleigh--Benard (RB) convection. RB configuration has attracted many researchers in view

of its natural and engineering occuring accessibility. In industries, the free air cooling due to RB convection happens from small scale computer chips to large scale processes that controls the quantity of excess heat from the system in order to achieve the longevity of equipment life. Owing to the wide applications, works on natural convection heated from below inside the cavity is found in literature [3–7].

The fluids suspended by nanoparticles known as nanofluids having higher thermal conductivity are considered as a promising technique to generate the higher heat transfer rate inside the cavity. [8] first examined the natural convection heat transfer enhancement utilizing nanofluids in a two dimensional rectangular cavity. They observed that the heat transfer rate increases due to the increase in the solid volume fraction of nanoparticles. The heat transfer behavior of copper-water nanofluids due to laminar natural convection characteristics in a differentially heated square cavity was studied by [9]. [10] performed the numerical simulation to study the flow and heat transfer characteristics of alumina-water nanofluid in a square cavity. [11] observed that the heat transfer performance is significantly affected by the inclination angle inline with nanofluid when the heater is placed either at a side wall or at corners of the cavity.

The configuration based on a square cavity with the presence of internal disturbance such as blocks in the study of heat and fluid flow has drawn great attention by many researchers due to its various practical applications. These include grain storages, heat exchangers and radiators, solidifications, cooling of microelectronic equipments, etc. [12] studied the natural convection fluid flow and heat transfer of copper-water nanofluid in a cavity having adiabatic square blockage at the center. Their study reported that at the low Rayleigh number, the size of the blockage has a significant effect on the heat transfer rate, whereas at a high Rayleigh number the size of blockage does not influenced the rate of heat transfer. [13] studied the heat transfer enhancement and entropy generation due to laminar natural convection in a differentially heated cavity with different types of blocks inside by the finite volume method. They found that when an isothermal cold blockage is placed inside the cavity, the heat transfer rate increased continuously with increase of the block size for the low Rayleigh number. [14] noted that the placement of blockages ensued different intensities of heat transfer inside the cavity. The numerical simulation of natural convection heat transfer of $Al_2O_3$-water nanofluid having an internal blockage inside the L-shaped cavity was considered by [15]. [16] studied the conjugate heat transfer analysis of natural convection filled with nanofluid in a partitioned cavity. They observed that by increasing the Grashof number and decreasing the Hartmann number, the local and average heat transfer rate was increased. Convective heat transfer in a rotating nanoliquid chamber with an isothermal heater located on the cavity was investigated by [17] employing the single-phase approach. [18] studied the influence of $\gamma\, Al_2O_3 - H_2O$ nanofluid in a square cavity with different shaped multiple obstacles. They noted the maximum heat transfer rate by considering the triangular obstacles.

With various applications of engineering, science and medicine such as in MHD power generators, oil separation and recovery from oil-contaminated sea water, and

drug industries, studies about magnetohydrodynamics emerged as a potential topic of interest in recent years. When the cavity is enriched with electrically conducting fluids, effect of the Lorentz force becomes active due to presence of the magnetic field and interacts with buoyancy force thereby influencing the flow and temperature fields. A detailed review on natural convective heat transfer of nanofluid filled cavities with magnetic field is summarized by [19]. The effect of a magnetic field on natural convection in a nanofluid filled cavity was examined by various researchers [20–25]. To the best of an author's knowledge, there have been no studies in the literature on the analysis of momentum and heat transport of RB convection in a square cavity with isothermal blockage under the influence of a uniform magnetic field. The present work focus to propose the two dimensional numerical solution by considering alumina-water nanofluid as the working fluid inside the cavity.

## 2. Mathematical formulation

The natural convection in a square cavity filled with an electrically conducting $Al_2O_3$ water nanofluid is considered with the presence of centrally positioned isothermally heated square blockage inside the cavity. The domain of the present study along with important geometrical parameters is shown in Figure 1. The length of the cavity is taken as H. An isothermally heated square blockage of size $B = D/H$ where $D = H/4$ is placed at the centre of the cavity. The blockage is maintained with temperature $(T_h + T_c)/2$ so that the blockage is produced with a uniform temperature inside the cavity. The top wall and partially heated bottom wall of the cavity are maintained with temperatures $T_c$ and $T_h$ respectively, while the remaining portions of the cavity is kept adiabatic. The directions of the acceleration due to gravity $g$ acts vertically downwards, and the velocity components $(u,v)$ are chosen along the cartesian coordinates $(x,y)$. The flow is considered unsteady, laminar, incompressible and two-dimensional. The thermal equilibrium is considered with the base fluid and nanoparticles. A uniform inclined magnetic field of constant magnitude $B_0$ is applied by forming an angle $\gamma$ with the horizontal axis.

The non-dimensional variables and parameters introduced to normalize the dimensional equations are given by:

$$X = \frac{x}{H},\ Y = \frac{y}{H},\ U = \frac{uH}{\alpha_f},\ V = \frac{vH}{\alpha_f},\ P = \frac{pH^2}{\rho_{nf}\alpha_f^2},\ \tau = \frac{t\alpha_f}{H^2},$$
$$\theta = \frac{T - T_c}{T_h - T_c},\ Pr = \frac{\nu_f}{\alpha_f},\ Ra = \frac{g\beta_f(T_h - T_c)H^3}{\nu_f\alpha_f},\ Ha = B_0 H\sqrt{\frac{\sigma_f}{\mu_f}}$$

With the above consideration, the governing non-dimensional equations for conservation of mass, momentum and energy together are given by:

$$\frac{\partial U}{\partial X} + \frac{\partial V}{\partial Y} = 0 \tag{1}$$

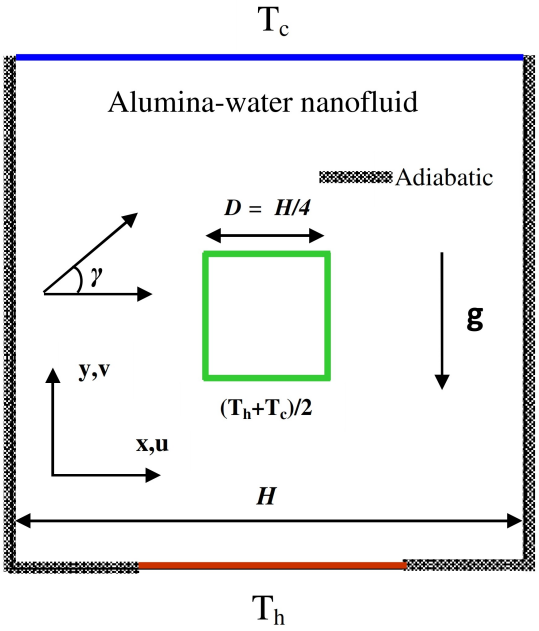


Fig. 1. Physical configuration

$$\frac{\partial U}{\partial \tau}+U\frac{\partial U}{\partial X}+V\frac{\partial U}{\partial Y}=-\frac{\partial P}{\partial X}+\frac{\mu_{nf}}{\rho_{nf}\alpha_f}\left(\frac{\partial^2 U}{\partial X^2}+\frac{\partial^2 U}{\partial Y^2}\right)$$
$$+\frac{\sigma_{nf}}{\sigma_f}\frac{\rho_f}{\rho_{nf}}Ha^2 PrV\sin\gamma\cos\gamma-\frac{\sigma_{nf}}{\sigma_f}\frac{\rho_f}{\rho_{nf}}Ha^2 PrU\sin^2\gamma \quad (2)$$

$$\frac{\partial V}{\partial \tau}+U\frac{\partial V}{\partial X}+V\frac{\partial V}{\partial Y}=-\frac{\partial P}{\partial Y}+\frac{\mu_{nf}}{\rho_{nf}\alpha_f}\left(\frac{\partial^2 V}{\partial X^2}+\frac{\partial^2 V}{\partial Y^2}\right)+\frac{(\rho\beta)_{nf}}{\rho_{nf}\beta_f}RaPr\theta$$
$$+\frac{\sigma_{nf}}{\sigma_f}\frac{\rho_f}{\rho_{nf}}Ha^2 PrU\sin\gamma\cos\gamma-\frac{\sigma_{nf}}{\sigma_f}\frac{\rho_f}{\rho_{nf}}Ha^2 PrV\cos^2\gamma \quad (3)$$

$$\frac{\partial \theta}{\partial \tau}+U\frac{\partial \theta}{\partial X}+V\frac{\partial \theta}{\partial Y}=\frac{\alpha_{nf}}{\alpha_f}\left(\frac{\partial^2 \theta}{\partial X^2}+\frac{\partial^2 \theta}{\partial Y^2}\right) \quad (4)$$

The non-dimensional form of initial and boundary conditions are given by:
$\tau = 0$: $U = 0, V = 0, \theta = 0.$
$\tau > 0$:
At left and right walls: $U = 0, V = 0, \dfrac{\partial \theta}{\partial X} = 0$
At top wall: $U = 0, V = 0, \theta = 0$
At bottom wall: $U = 0, V = 0$, Active part: $\theta = 1$, Remaining part: $\dfrac{\partial \theta}{\partial Y} = 0$
At blockage: $U = 0, V = 0, \theta = 0.5$.

The thermophysical properties such as effective density $\rho_{nf}$, thermal expansion coefficient $(\rho\beta)_{nf}$, thermal conductivity $k_{nf}$, heat capacitance $(\rho C_p)_{nf}$, electrical

conductivity $\sigma_{nf}$, thermal diffusivity $\alpha_{nf}$ and dynamic viscosity $\mu_{nf}$ of the nanofluid are defined as below:

$$\begin{aligned}
\rho_{nf} &= (1-\phi)\rho_f + \phi\rho_s, \quad (\rho\beta)_{nf} = (1-\phi)(\rho\beta)_f + \phi(\rho\beta)_s \\
\frac{k_{nf}}{k_f} &= \frac{k_s + 2k_f - 2\phi(k_f - k_s)}{k_s + 2k_f + \phi(k_f - k_s)}, \quad (\rho C_p)_{nf} = (1-\phi)(\rho C_p)_f + \phi(\rho C_p)_s \\
\sigma_{nf} &= \sigma_f\left[1 + \frac{3(\frac{\sigma_s}{\sigma_f} - 1)\phi}{(\frac{\sigma_s}{\sigma_f} + 2) - (\frac{\sigma_s}{\sigma_f} - 1)\phi}\right], \quad \alpha_{nf} = \frac{k_{nf}}{(\rho C_p)_{nf}}, \quad \mu_{nf} = \frac{\mu_f}{(1-\phi)^{2.5}}
\end{aligned}$$

where $\phi$ is the solid volume fraction of the nanoparticles.

The expression for the local Nusselt number is given by

$$Nu_{loc} = \frac{hH}{k_f}$$

where the heat transfer coefficient and thermal conductivity are given by

$$h = \left.\frac{q_w}{T_h - T_c}\right|_{y=0} \quad k_{nf} = -\frac{q_w}{\partial T/\partial y}$$

The heat transfer coefficient in terms of local Nusselt number $Nu_{loc}$ and average Nusselt number $Nu_{avg}$ is given by

$$Nu_{loc} = -\left(\frac{k_{nf}}{k_f}\right)\left.\frac{\partial\theta}{\partial Y}\right|_{Y=0} \qquad Nu_{avg} = \int_{\frac{(1-\varepsilon)}{2}}^{\frac{(1+\varepsilon)}{2}} Nu_{loc}\,\mathrm{d}X$$

## 3. Numerical methodology

The unsteady non-dimensional Eqs. (1)-(4) together with the boundary conditions are numerically solved using the finite volume method (FVM). In this method, the unsteady non-dimensional equations are integrated over the finite number of control volumes and time steps. A staggered grid refinement is chosen to store the scalar variables at the main nodal points and the vector quantities at the cell faces of the control volumes. The power law scheme and central differencing scheme are respectively used to approximate the convective and diffusive terms. The SIMPLE (Semi-Implicit Method for Pressure Linked Equation) algorithm of [26] is taken to solve the coupling of continuity and pressure velocity equations. The non-dimensional equations are converted into a system of algebraic equations and solved using the Thomas algorithm. The method is repeated continuously until the following convergence norm is satisfied:

$$\left|\frac{\varphi^{n+1}(i,j) - \varphi^{n}(i,j)}{\varphi^{n+1}(i,j)}\right| \leq 10^{-5}$$

Here $\varphi$ corresponds to velocities $U$, $V$ and temperature $\theta$, while $n$ is any time level and $(i, j)$ indicates the space co-ordinates.

The numerical tests are performed with structured sized grid points of $20 \times 20$ to $160 \times 160$ to obtain results for the average Nusselt number at fixed Ra = $10^5$, $\phi = 0.02$ and B = 0.25 as shown in Figure 2a. The mesh generation of computational domain is presented in Figure 2b. It is seen from the figure that the average Nusselt number does not change after the higher grid dimension of $120 \times 120$. Hence, to reduce the complexity in the computational domain a uniform grid system of $120 \times 120$ is used in the present study for the calculation of all cases.

In order to check the validity of the developed code, a numerical comparison is conducted with the published results of [20] for horizontal velocity (Fig. 3a) and vertical velocity (Fig. 3b). Also, the streamlines (Fig. 3c) and isotherms (Fig. 3d) at $Ra = 10^6$ is compared with B = 0.25 with the work of [13]. A matchable agreement is obtained from the figure which gives good confidence to the numerical outcome of the present study to be discussed in the next section.

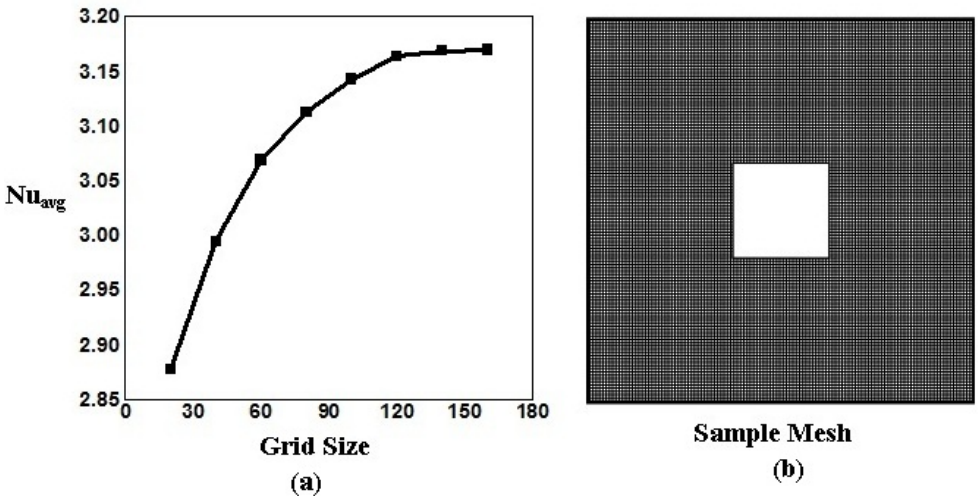


Fig. 2. Grid independence test (a), sample mesh of computational domain (b)

## 4. Results and discussion

In this section, the numerical simulation is performed to understand the magnetoconvection heat and fluid flow of $Al_2O_3$ water nanofluid in a partially heated bottom cavity with isothermal heated blockage inside. The study is carried out by varying the following parameters such as Rayleigh number ($Ra = 10^4$-$10^6$), Hartmann number ($Ha =$ 10-500), inclination angle of magnetic field ($\gamma = 0^\circ$-$90^\circ$), length of heat source ($\varepsilon =$ 0.25-1.0) and size of blockage ratio ($B =$ 0.25-0.75). The Prandtl number ($Pr$) and solid volume fraction of nanoparticles ($\phi$) are fixed at 6.2 and 0.02 respectively throughout the study. The results are analyzed in the form of streamlines,

isotherms, mid height velocity profiles and the rate of heat transfer using suitable plots.

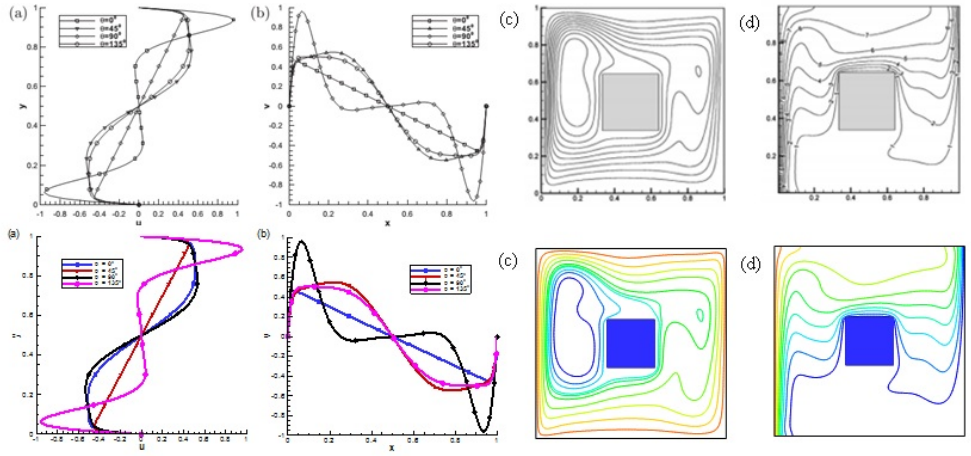


Fig. 3. Comparison of (a) horizontal velocity, (b) vertical velocity for different inclination angle with work of [20] and (c) streamlines, (d) isotherms for $Ra = 10^6$ with work of [13]

Figure 4 represent streamlines and isotherms contours for different $Ra$ and $\gamma$ at fixed $Ha = 50, \varepsilon = 0.5$ and $B = 0.25$. When the magnetic field is not inclined ($\gamma = 0^\circ$), the application of inclined magnetic field acts along the direction normal to the vertical walls of the cavity. At $Ra = 10^4$, streamlines are formed with multicellular flow patterns of anticlockwise and clockwise rotating cells emerged along the left and right sides of the blockage respectively inside the cavity. When the Rayleigh number is increased to $10^5$, the flow fields changed such that the clockwise rotating eddies influenced the major regions of the cavity. A further increase in the $Ra$ creates dominant buoyancy force and results in the formation of anticlockwise and clockwise rotating cells with high flow rates around the left and right sides of the heated body respectively in equal proportions inside the cavity. For all $\gamma$, temperature fields corresponds to conduction mode of heat transfer at $Ra = 10^4$ inside the cavity. When $\gamma$ is increased to $30^\circ$, the anticlockwise rotating eddies elongated by suppressing the clockwise rotating cells towards the right wall for $Ra = 10^4$. At $Ra = 10^5$, flow circulation develops with the formation of oval shaped vortices of anticlockwise eddies developed at the bottom left and top right corners of the heated body while the clockwise rotating eddies emerged at the top left and bottom right corners of the cavity. At $Ra = 10^6$, the high effect of buoyancy force together with the inclined magnetic field changes the streamlines flow patterns such that the anticlockwise rotating cells are formed in three layers (i.e.) the first layer gets crowded in the circular pattern around the heated blockage, the second layer with circulating vortices at the four corners, and the third layer, formed in rectangular form inside the cavity. A further increase in inclination angle corresponds to the primary and secondary cells to occupy almost equal spaces around the heated blockage for $Ra = 10^4$ but at

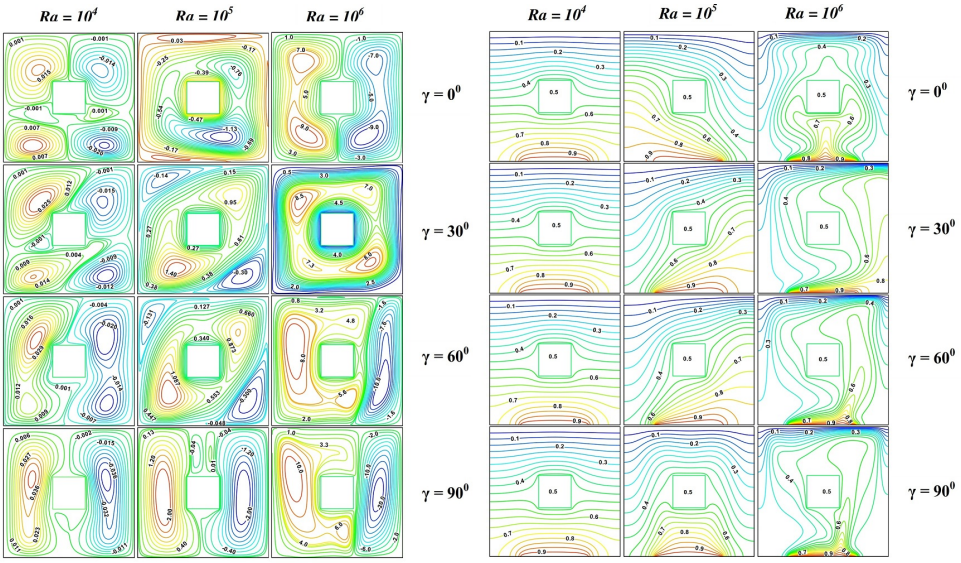


(a) (b)

Fig. 4. Streamlines (a) and isotherms (b) for different $Ra$ and $\gamma$ at fixed $Ha = 50$, $\varepsilon = 0.5$ and $B = 0.25$

$Ra = 10^5$, vortices become more inclined at their respective regions inside the cavity. At $Ra = 10^6$, counter-rotating eddies contracts towards the heated blockage, and the clockwise rotating eddies are developed towards the right side of heated blockage inside the cavity. At $\gamma = 90^\circ$, the vertically applied magnetic field separated patterns of anticlockwise and clockwise rotating cells towards the left and right sides of the heated blockage inside the cavity for all Ra. At $Ra = 10^5$, the temperature contours emerged about the heated portion of bottom wall and approached towards the left corner indicating the quasi-conduction heat transfer mode. At $Ra = 10^6$, the effect of increased buoyancy force resulted in the distribution of isotherms patterns and resembled convective heat transfer inside the cavity.

The influence of the different blockage ratio and inclination angle on streamlines and isotherms at fixed $Ha = 50, \varepsilon = 0.5$ and $Ra = 10^5$ is demonstrated in Figure 5. At $\gamma = 0^\circ$ and for $B = 0.125$, streamlines are developed with high flow rates of counter-clockwise and clockwise rotating cells inside the cavity. When $\gamma$ is further increased, the effect of inclined magnetic field acting in either direction tends the anti-clockwise and clockwise patterns of streamlines much more inclined at the respective regions in the cavity. At $\gamma = 90^\circ$, clockwise and counter-rotating eddies are produced with opposite mirror images and are almost parallel to the vertical boundaries of the cavity due to the applied magnetic field along vertical direction. The corresponding isotherms contours developed from the bottom right regions of the heated wall and reached along vertical boundaries representing the conduction-convection heat transfer mode inside the cavity for $\gamma \leq 60^\circ$. At $\gamma = 90^\circ$, the temperature contours are almost parallel towards the horizontal boundaries of the cavity.

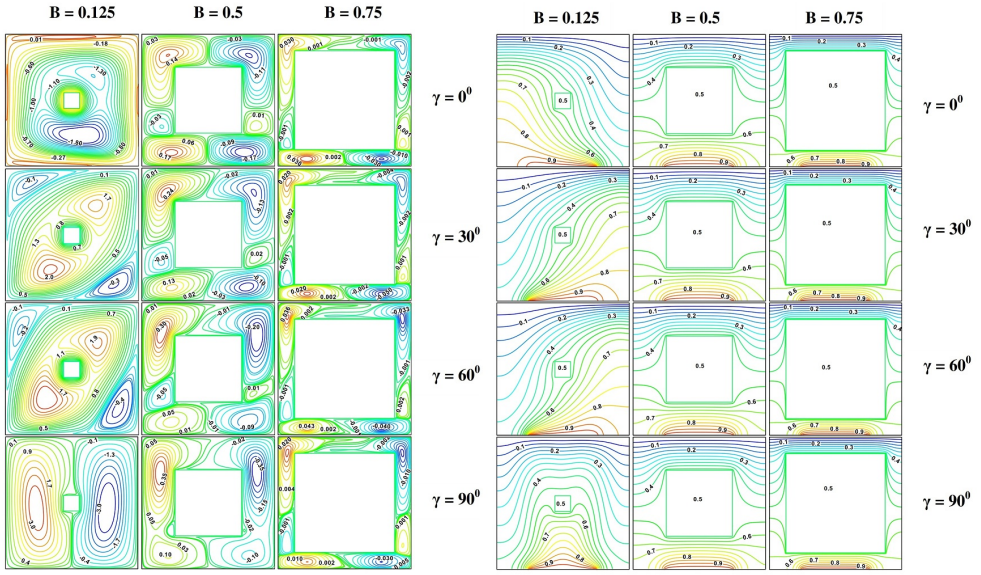


Fig. 5. Streamlines (a) and isotherms (b) for various $B$ and $\gamma$ at fixed $Ha = 50$, $\varepsilon = 0.5$ and $Ra = 10^5$

At $B = 0.5$, the effect of inclined magnetic field is nullified due to the increment in size of isothermal heated blockage, and slight changes on streamlines patterns are observed for $\gamma \leq 60^{\circ}$. For $\gamma = 90^{\circ}$, streamlines are formed with opposite mirror images around the heated body inside the cavity. For $B = 0.75$, the effect of varying $\gamma$ has no significant influence on streamlines due to the occupancy of $B$ such that streamlines emerged with multicellular flow patterns of clockwise and anticlockwise eddies inside the cavity for all $\gamma$. The isothermal lines indicated the conductive mode of heat transfer inside the cavity for all $\gamma$.

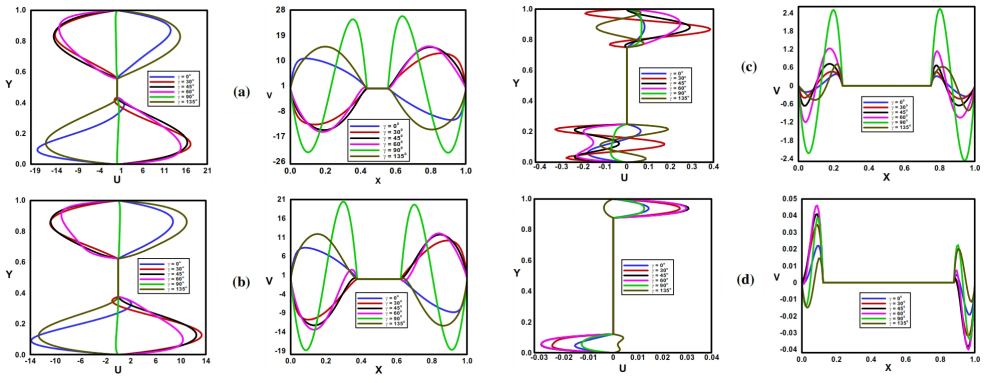


Fig. 6. Mid height horizontal and vertical velocity profile for different $\gamma$ and (a) $B = 0.125$, (b) $B = 0.25$, (c) $B = 0.5$ and (d) $B = 0.75$ at fixed $\varepsilon = 0.5, Ha = 50$ and $Ra = 10^5$

The mid height horizontal and vertical velocity profiles for different $\gamma$ and $B$ at fixed $\varepsilon = 0.5$, $Ha = 50$ and $Ra = 10^5$ is shown in Figure 6. It is observed that when the inclined magnetic field is kept at 90°, the minimum vertical velocity and maximum horizontal velocity are observed inside the cavity.

Figure 7 represents the local Nusselt number for different $\varepsilon$ and $\gamma$ at fixed values of $Ha = 50$, $Ra = 10^5$ and $B = 0.25$. For the length of heat source in the range $0.25 \leq \varepsilon \leq 0.75$, the local heat transfer rate is found to be maximum at the right end of the heat source length ($\gamma = 0°$), at the left end of the heat source length ($\gamma = 30°, 60°$) and at the both ends of the heat source length ($\gamma = 90°$), respectively. When $\varepsilon = 1.0$, the local Nusselt number decreases from the left end to the right end of the bottom wall for $\gamma = 0°$, whereas for $\gamma = 30°$ and 60°, the local Nusselt number increases at the first half of the heated portion of wall and then decreases. At $\gamma = 90°$, the heat transfer rate decreases at the center half of the heated wall and then increases.

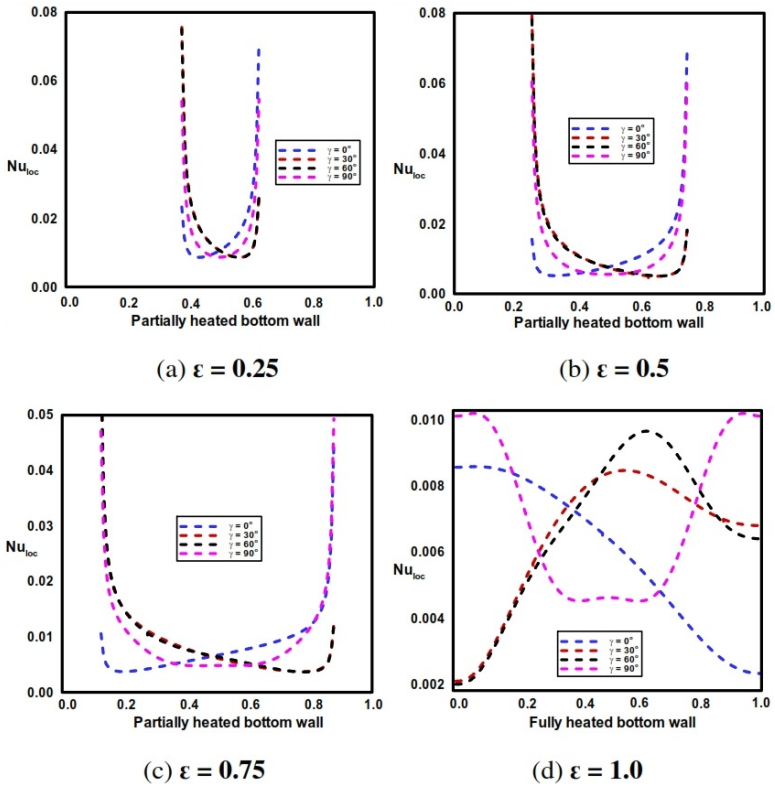


Fig. 7. Local Nusselt number for different $\gamma$ and different (a) $\varepsilon$ = 0.25, (b) $\varepsilon$ = 0.5, (c) $\varepsilon$ = 0.75 and (d) $\varepsilon$ = 1.0 at fixed $Ha$ = 50, $B$ = 0.25 and $Ra = 10^5$

Figure 8 shows the local heat transfer rate of the partially heated bottom wall for the different $B$ and $\gamma$ at fixed $\varepsilon = 0.5$, $Ra = 10^5$ and $Ha = 50$. At $B = 0.125$ and $\gamma = 0°$, a slight decrease in the local Nusselt number is observed along the left end of the heated wall and then the local Nusselt number increases and is found to be

maximum at the right end of the heated wall. When increasing $\gamma$ to 30° and 60°, a contrast behavior to $\gamma = 0°$ is witnessed. At $\gamma = 90°$, the local Nusselt number is maximum at both ends of the heated wall. For $B = 0.5$, it is noticed that the local Nusselt number decreases at both ends and becomes flat at the middle region on the active bottom wall of the cavity.

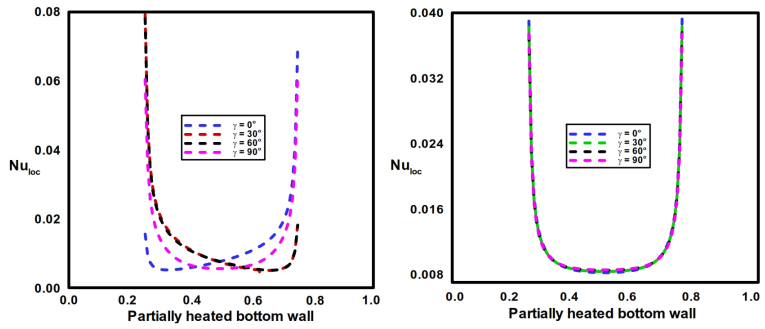


Fig. 8. Local Nusselt number for different $\gamma$ and different (a) $B = 0.125$ and (b) $B = 0.5$ at fixed $Ha = 50$, $\varepsilon = 0.5$ and $Ra = 10^5$

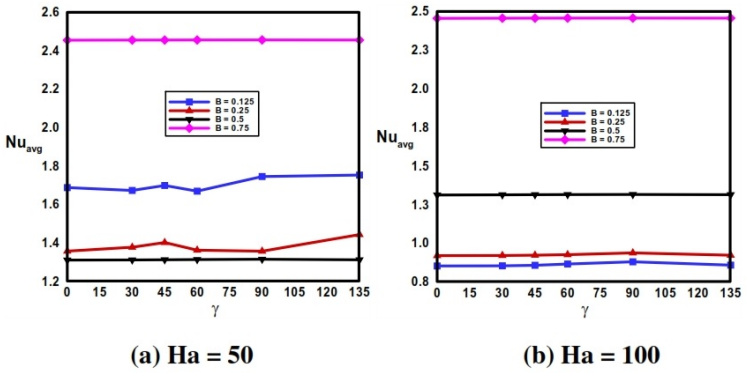


Fig. 9. Average Nusselt number for different $B$ and $\gamma$ at fixed Hartmann number (a) $Ha = 50$, (b) $Ha = 100$ and fixed $\varepsilon = 0.5$ and $Ra = 10^5$

Figure 9 indicates the plot of average Nusselt number for different $B$ and $\gamma$ at fixed $\varepsilon = 0.5$, $Ra = 10^5$ for $Ha = 50$ and $Ha = 100$. At $Ha = 50$, for the small size of blockage, the average heat transfer rate is minimum at $\gamma = 0°$ and is found to be high at $\gamma = 90°$. When $B$ is increased to 0.25 and 0.5, the average Nusselt number decreases. When the dimension ratio is further increased, the blockage occupying the three-fourth region inside the cavity opposes the effect of the magnetic field produced by the $Ha$, and the maximum heat transfer rate is observed for the dimension ratio

for all the values of $\gamma$. At $Ha = 100$, the average heat transfer rate is found to be minimum for all values of $\gamma$ for the dimension ratio $B = 0.125$. When increasing the dimension ratio, the average heat transfer also increases, and the maximum heat transfer is observed for $B = 0.75$ and it remains almost constant for all $\gamma$.

The average Nusselt number for different $Ra$ and $\gamma$ at fixed $\varepsilon = 0.5$, $Ha = 50$ and $B = 0.25$ is demonstrated in Figure 10a. For low values of $Ra = 10^3$ and $Ra = 10^4$, the least effect caused by the buoyancy force produces the minimum heat transfer rate inside the cavity and is identical for all $\gamma$. When $Ra$ is increased, the rise in the buoyancy force increases $Nu_{avg}$. The maximum heat transfer rate is observed for $Ra = 10^6$ at $\gamma = 90^\circ$.

Figure 10b shows the heat transfer rate for different $Ha$ and $\gamma$ at fixed $\varepsilon = 0.5$, $Ra = 10^5$ and $B = 0.25$. The high buoyancy force at $Ra = 10^5$ is not largely affected by low value of $Ha = 10$, and the maximum average heat transfer is experienced. When increasing $Ha$ to 50, the growth in the magnetic field retarded the buoyancy force and the maximum heat transfer rate is produced by fixing $\gamma$ at 45°.The increase in magnetic field by increasing $Ha$ decreases $Nu_{avg}$ and remains the same for all $\gamma$.

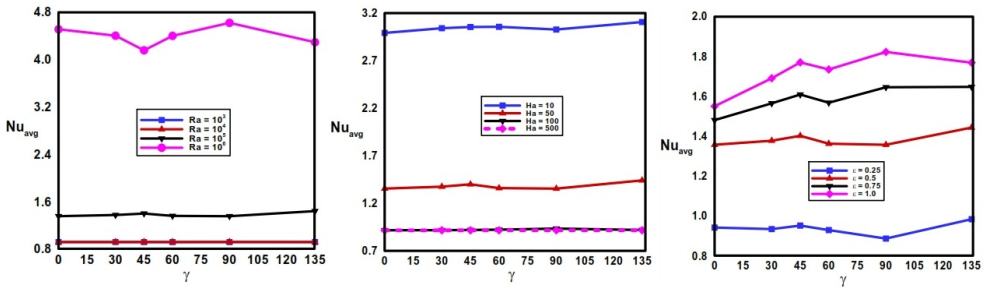


Fig. 10. $Nu_{avg}$ for different $\gamma$ at (a) different $Ra$ at fixed $\varepsilon = 0.5$, $Ha = 50$ and $B = 0.25$, (b) different $Ha$ at fixed $\varepsilon = 0.5$, $B = 0.25$ and $Ra = 10^5$, (c) different $\varepsilon$ at fixed $B = 0.25$, $Ha = 50$ and $Ra = 10^5$

The $Nu_{avg}$ for different $\varepsilon$ and $\gamma$ at fixed $Ha = 50$, $Ra = 10^5$ and $B = 0.25$ is depicted in Figure 10c. When the length of bottom heater is kept small ($\varepsilon = 0.25$ and $\varepsilon = 0.5$), the maximum and minimum heat transfer are noted for $\gamma$ at 45° and 90°, respectively. When the heater length is increased above 0.5, $Nu_{avg}$ is found to be low for the vertically inclined magnetic field ($\gamma = 0^\circ$) and high for the horizontally inclined magnetic field ($\gamma = 90^\circ$).

## 5. Conclusions

The natural convection heat transfer of water based $Al_2O_3$ nanofluid with isothermal square blockage in a partially heated cavity under the influence of uniform magnetic field is examined. From this study, the following remarks can be concluded:

- The flow and temperature fields are significantly influenced by the dimensionless parameters. Moreover, at $\gamma = 90^{\circ}$, the flow fields are almost parallel to the vertical boundaries of the cavity, and the convection heat transfer mode is noticed for large values of $Ra$, small values of $Ha$ and $B$.
- The local heat transfer rate is found to be maximum at both ends of the heated bottom wall for $\gamma = 90^{\circ}$.
- At $\varepsilon = 0.25$ and $\varepsilon = 0.5$, the average heat transfer rate is found to be high at $\gamma = 45^{\circ}$.
- The $Nu_{avg}$ is maximum for small $Ha$ at $\gamma = 45^{\circ}$. The $Nu_{avg}$ is found to be low and are same throughout for higher $Ha$ for all the values of $\gamma$.
- The higher heat transfer rate is observed for the larger Rayleigh number at $\gamma = 90^{\circ}$.
- When varying $B$, the higher heat transfer rate is obtained for $B = 0.75$ for all $\gamma$ due to the domination of isothermal blockage inside the cavity.

## References


[1] Memon, A.G., & Memon, R.A. (2017). Thermodynamic analysis of a trigeneration system proposed for residential application. *Energy Conversion and Management*, *145*, 182-203.

[2] Saleem, K.B., Koufi, L., Alshara, A.K., & Kolsi, L. (2020). Double-diffusive natural convection in a solar distiller with external fluid stream cooling. *International Journal of Mechanical Sciences*, *181*, 105728.

[3] Ridouane, E.H., Hasnaoui, M., Amahmid, A., & Raji, A. (2004). Interaction between natural convection and radiation in a square cavity heated from below. *Numerical Heat Transfer, Part A: Applications*, *45*, 289-311.

[4] Lyubimov, D.V., Kovalevskaya, K.V., & Lyubimova, T.P. (2012). Bifurcation analysis of a viscoelastic fluid heated from below. *Communications in Nonlinear Science and Numerical Simulation*, *17*, 3521-3532.

[5] Nasseri, L., Himrane, N., Ameziani, D.E., Bourada, A., & Bennacer, R. (2021). Time-periodic cooling of Rayleigh-Benard convection. *Fluids*, *6*, 1-15.

[6] Ganesh, N.V., Al-Mdallal, Q.M., Oztop, H.F., & Kalaivanan, R. (2021). Analysis of natural convection for a Casson-based multiwall carbon nanotube nanofluid in a partially heated wavy enclosure with a circular obstacle in the presence of thermal radiation. *Journal of Advanced Research*.

[7] Ganesh, N.V., Al-Mdallal, Q.M., Hirankumar, G., Kalaivanan, R., & Chamkha, A.J. (2021). Buoyancy-driven convection of MWCNT-Casson nanofluid in a wavy enclosure with a circular barrier and parallel hot/cold fins. *Alexandria Engineering Journal*, *61*, 3249-3264.

[8] Khanafer, K., Vafai, K., & Lightstone, M. (2003). Buoyancy-driven heat transfer enhancement in a two-dimensional enclosure utilizing nanofluids. *International Journal of Heat and Mass Transfer*, *46*, 3639-3653.

[9] Santra, A.K., Sen, S., & Chakraborty, N. (2008). Study of heat transfer characteristics of copper-water nanofluid in a differentially heated square cavity with different viscosity models. *Journal of Enhanced Heat Transfer*, *15*, 273-287.

[10] Rashidi, I., Mahian, O., Lorenzini, G., Biserni, C., & Wongwises, S. (2014). Natural convection of $Al_2O_3$/water nanofluid in a square cavity: Effects of heterogeneous heating. *International Journal of Heat and Mass Transfer*, *74*, 391-402.

[11] Emami, R.Y., Siavashi, M., & Moghaddam, G.S. (2018). The effect of inclination angle and hot wall configuration on Cu-water nanofluid natural convection inside a porous square cavity. *Advanced Powder Technology*, *29*, 519-536.

[12] Mahmoodi, M., & Sebdani, S.M. (2012). Natural convection in a square cavity containing a nanofluid and an adiabatic square block at the center. *Superlattices and Microstructures*, *52*, 261-275.

[13] Mahapatra, P.S., De, S., Ghosh, K., Manna, N.K., & Mukhopadhyay, A. (2013). Heat transfer enhancement and entropy generation in a square enclosure in the presence of adiabatic and isothermal blocks. *Numerical Heat Transfer, Part A*, *64*, 1-20.

[14] Kalidasan, K., Velkennedy, R., & Kanna, P.R. (2016). Natural convection heat transfer enhancement using nanofluid and time-variant temperature on the square enclosure with diagonally constructed twin adiabatic blocks. *Applied Thermal Engineering*, *92*, 219-235.

[15] Mohebbi, R., & Rashidi, M.M. (2017). Numerical simulation of natural convection heat transfer of a nanofluid in an L-shaped enclosure with a heating obstacle. *Journal of the Taiwan Institute of Chemical Engineers*, *72*, 70-84.

[16] Selimefendigil, F., & Oztop, H.F. (2018). *MHD natural convection and entropy generation in a nanofluid-filled cavity with a conductive partition. In: Exergetic, Energetic and Environmental Dimensions* (pp. 763-778). Academic Press.

[17] Mikhailenko, S.A., Sheremet, M.A., Oztop, H.F., & Abu-Hamdeh, N. (2019). Thermal convection in $Al_2O_3$–water nanoliquid rotating chamber with a local isothermal heater. *International Journal of Mechanical Sciences*, *156*, 137-145.

[18] Ganesh, N.V., Javed, S., Al-Mdallal, Q.M., Kalaivanan, R., & Chamkha, A.J. (2020). Numerical study of heat generating $\gamma Al_2O_3 - H_2O$ nanofluid inside a square cavity with multiple obstacles of different shapes. *Heliyon*, *6*, e05752.

[19] Molana, M., Zarrinderafsh, V., Chamkha, A.J., Izadi, S., & Rafizadeh, S. (2020). Magnetohydrodynamics convection in nanofluids-filled cavities: A review. *Heat Transfer*, *49*, 1418-1443.

[20] Yu, P.X., Qiu, J.X., Qin, Q., & Tian, Z.F. (2013). Numerical investigation of natural convection in a rectangular cavity under different directions of uniform magnetic field. *International Journal of Heat and Mass Transfer*, *67*, 1131-1144.

[21] Al-Zamily, A.M.J. (2014). Effect of magnetic field on natural convection in a nanofluid-filled semi-circular enclosure with heat flux source. *Computers & Fluids*, *103*, 71-85.

[22] Malvandi, A., & Ganji, D.D. (2015). Magnetic field and slip effects on free convection inside a vertical enclosure filled with alumina/water nanofluid. *Chemical Engineering Research and Design*, *94*, 355-364.

[23] Miroshnichenko, I.V., Sheremet, M.A., Oztop, H.F., & Al-Salem, K. (2016). MHD natural convection in a partially open trapezoidal cavity filled with a nanofluid. *International Journal of Mechanical Sciences*, *119*, 294-302.

[24] Al Kalbani, K.S., Rahman, M.M., Alam, S., Al-Salti, N., & Eltayeb, I.A. (2018). Buoyancy induced heat transfer flow inside a tilted square enclosure filled with nanofluids in the presence of oriented magnetic field. *Heat Transfer Engineering*, *39*, 511-525.

[25] Li, Z., Shafee, A., Ramzan, M., Rokni, H.B., & Al-Mdallal, Q.M. (2019). Simulation of natural convection of $Fe_3O_4$-water ferrofluid in a circular porous cavity in the presence of a magnetic field. *European Physical Journal Plus*, *134*, 1-8.

[26] Patankar, S.V. (1980). *Numerical Heat Transfer and Fluid Flow*. CRC Press.